Sensor Fusion for Position Estimation in Robot-based Laser Material Processing

Philipp Walderich[1], Leon Gorissen[1], Thomas Kaster[1], and Christian Hinke[1]

[1]*Chair for Laser Technology – RWTH Aachen University, Steinbachstr. 15, 52074 Aachen, Germany*
[*]*Corresponding author's e-mail: philipp.walderich@llt.rwth-aachen.de*

Abstract – This paper investigates an Extended Kalman Filter (EKF) based Sensor Fusion approach for robot tool center point (TCP) position estimation using a sensing unit consisting of multiple sensors. Data from an inertial measurement unit, axis encoders and two new optical sensors for relative speed estimation in the context of laser material processing is recorded. Performance of the approach is tested experimentally. Three different test trajectories are chosen to evaluate estimation performance, including an adaption of ISO 9283 trajectory for robot accuracy. Estimation results are compared to position measurements of a Laser Tracker system with measurement accuracy of +-28µm and position estimation of the robot controller of the used Universal Robots UR5e.

DOI: 10.2961/jlmn.2024.01.2013

Keywords: position estimation, sensor fusion, laser material processing

1. Introduction

Laser manufacturing processes (LMP) can yield high degrees of precision and flexibility and hence be used to manufacture complex and individualized products or parts. [1] Further, costs of kw laser beam sources decreased by up to 70%, reducing its share of costs for laser machines drastically**.** [2] Through use of low-cost industrial robots (IR) overall investment costs can be reduced and LMP could be made affordable for new user groups. IRs can be subject to different mechanical and thermal sources of error such as limited mechanical stiffness of the links or gearbox transmission errors as well as errors rooted in robot control or by the manufacturing process causing deviations from the intended process. [3, 10, 13] Effects of path accuracy on LMP results can be observed. For example, in robot-based Laser Material Deposition (LMD) influence of the path deviations on resulting product geometry is visible. Resulting geometry deviations of up to 0.24mm are observable for high precision IRs such as Kuka KR90 HA. [4] Hence, robot position accuracy must be improved to leverage the potential of robot-based LMP. To be able to control tool center point position (TCP) during laser manufacturing, a precise measurement of the deviation of the attained trajectory from the command trajectory is necessary at low costs. Therefore, a sensor fusion TCP position estimation approach is investigated in this paper.

2. Experimental Setup

2.1 System Setup

The proposed system makes use of a sensing unit depicted in Fig. 1. This sensing unit consists of an inertial measurement unit (IMU) and two optical VSCEL sensors (OS). Additionally rotary encoders of the industrial robot are recorded. The different sensors provide:

- Acceleration data (IMU)
- Translational velocity (OS),
- Joint position data (UR5e)

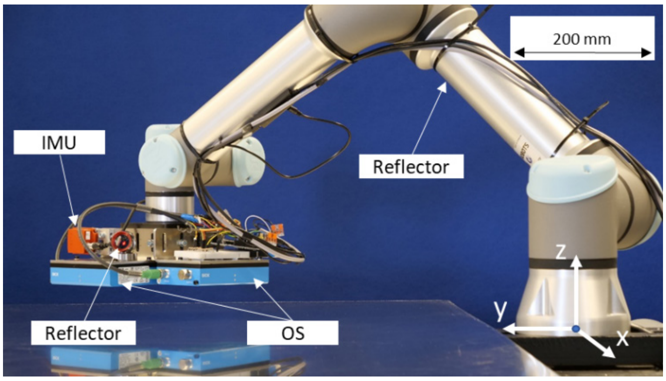

Fig. 1 Sensing unit mounted to robot with reflector of Laser Tracker system.

The IMU used is a MEMS IMU type MTi-30 of the brand Xsens Technologies B.V. The IMU has a spectral noise density of 72.5 $\mu g/\sqrt{Hz}$. According to the bandwidth of the IMU of 375 Hz the lower bound for the measurement resolution is given with 0.014 m/s^2 for measured accelerations. Measurements are taken with a frequency of 100 Hz. Optical VCSEL sensors used are type Speetec 1D by Sick AG. Measurement output is relative distance from initialization point. Velocity is calculated with according timestamps. According to manufacturer, measuring accuracy is 0.1% of speed, for a speed range of 0.2m/s-10m/s. Measurements are taken at 490 Hz. A working distance of 50mm±5mm must be maintained. The robot used is a Universal Robots UR5e six-axis IR. Joint position data of the UR5e robot required for the experiment are provided via the Real Time Data Exchange (RTDE) interface at 500Hz. Also, robot position data (RPD) in cartesian space is recorded. Information on measurement accuracy was not available by the manufacturer. As reference position measurement a Laser Tracker (LT) type AT930 by Hexagon Metrology GmbH is used to measure the actual position of the TCP during experiments. Position measurements are recorded with a maximum error of 28µm at 490Hz.

2.2 Experimental Design

Position estimation performance is evaluated for three different geometries at two constant feed rates. All experiments are executed in the xy-plane of the robot base frame (see. Fig 1) with a distance to the metal sheet of 50mm. Experimental evaluation is done in the same coordinate system. All motions start with a run-in route from P_0 to P_1. First test path is an isosceles triangle in which the orthogonal sides have a length of 50 mm to investigate performance at abrupt directions changes. Second test path is circle with a diameter of 100 mm account for more subtle but constant changes in direction.

In Fig. 2 triangular and circular motion are depicted.

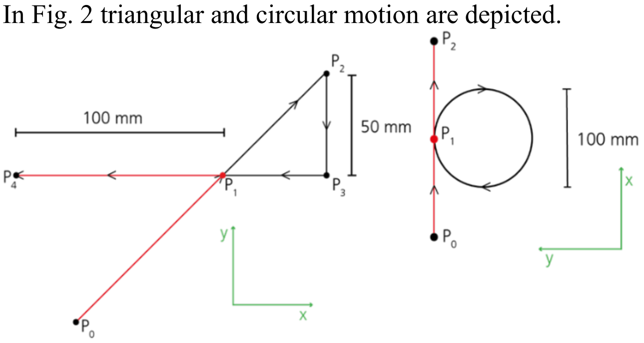

Fig. 2 Triangular and circular test paths.

In Fig. 3 an adaption of the ISO 9283 test path is depicted. Geometry is developed to create a closed contour in order to be used in experiments in which laser processes might be applied, e.g. laser cutting.

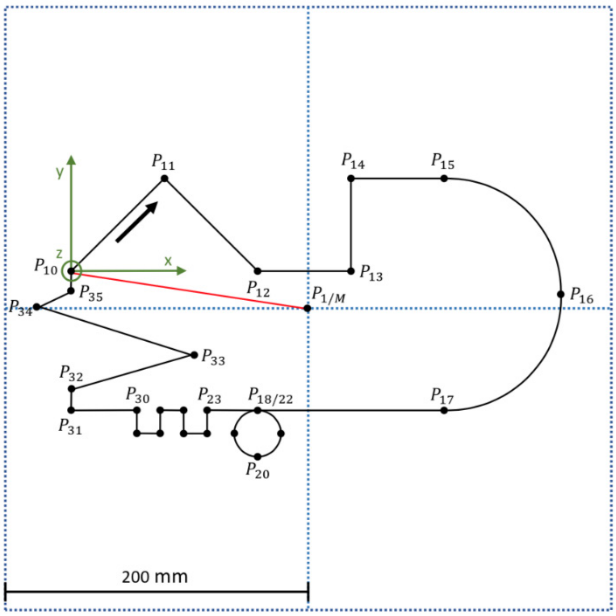

Fig. 3 Adapted ISO 9283 test path.

To be able to observe the influence of the velocity on the estimation results at abrupt direction changes, the triangular test path is conducted at two different feedrates. Feedrates chosen are $v_1 = 50$ mm/s and $v_2 = 150$ mm/s. Circular and iso paths are conducted at v_2. All experiments were run six times.

3. Methods

3.1 State Estimation

Sensor fusion uses data from multiple sensors to provide more accurate estimate of the system state [5]. This may be necessary when individual sensors are not sufficient to fully describe the state of a system because they provide limited information. Another reason is that sensors provide erroneous information, i.e., the readings are noisy or affected by other disturbances. The sensors are combined in such a way that the respective advantages compensate for the uncertainties as far as possible. For example, some sensors have low spatial resolution or measuring frequency. This is often the case with absolute measuring systems, such as the global navigation satellite system (GNSS) in terms of position determination for some applications. Relative-measurement sensors, such as IMUs, are compounded by the fact that they provide accurate position data locally and for short periods of time, but drift over longer measurement periods [6]. An SF can be used to fuse the above sensors and thus minimize the measurement uncertainties, as is currently used in autonomous driving vehicles [7]. The Extended Kalman Filter is a state estimator and represents an extended form of the linear Kalman Filter (LKF). With this variant of the Kalman Filter, non-linear systems can also be estimated. The LKF, as well as the EKF, are used in the following as a recursive Bayes estimator for systems with a Gaussian distributed system model. The filter is divided into two phases. In the first phase of the prediction, the current state is estimated based on the result of previous filter step using a system model and the input variables of the system. This state is called the a-priori estimate. In the next step, the correction step, the a priori estimate is combined with the measurements and an updated state estimate is calculated. This provides the a-posteriori estimate. The basic model of the recursive EKF consists of a system model:

$$x_{\mathrm{k}+1} = f(x_k, u_k, w_k) \tag{1}$$

which computes the a priori state vector $x_{\mathrm{k}+1}$ at time k+1. The variables x_{k}, u_{k} and w_{k} represent the a posteriori estimate of the previous state, the input vector and the noise of the process model. The measurement model $h(x_k)$ maps the state vector x_k to the measurement y_k. This is assigned an additive noise e_k.

$$y_k = h(x_k) + e_k \tag{2}$$

The noise quantities w_{k} and e_k are assumed to be mean-free Gaussian noise. The extension of the EKF in comparison to LKF is to linearize the nonlinear functions h and f around the current estimate $\hat{x}_k$. Here, the matrix F_j is the Jacobian of f:

$$F_J = \left.\frac{\partial f(\mathrm{x},\mathrm{u},\mathrm{w})}{\partial \mathrm{x}}\right|_{\hat{x}_k,\mathrm{u}} \tag{3}$$

Jacobian H of h is calculated analogously. [6]

The UR5e six axis articulated robot arm of which the kinematic chain consists of six rotational joints. The axis angles are stored in the vector:

$$\mathrm{q} = (\mathrm{q}^1 \quad \cdots \quad \mathrm{q}^6)^T \tag{4}$$

Robot state space is then given by:

$$x = (q \quad \dot{q} \quad \ddot{q})^T \in \mathbb{R}^{18} \tag{5}$$

The vectors $\dot{q}$ and $\ddot{q}$ are the angular velocity and angular acceleration of the joint axes. Since the reference measurement is in Cartesian space, the axis angles of the state vector are converted to a TCP position in Cartesian space via the forward kinematic transformation which describes the relative position of the axis coordinate systems of the robot joints for given joint positions. For this purpose, transformation matrices are determined with the help of Denavit-Hartenberg (DH)-parameters. In this classic notation the relations between two sequential robot axis coordinate systems is given by the distance along and rotation around z-axis (d and θ) and the x-axis (a and α) accordingly. By calculation of forward kinematics position of the TCP is calculated in cartesian space. [8,9] Following DH-parameters were read out from the robot-controller of the UR5e robot and given in Table 1:

Table 1 DH-parameters for FK calculation.

θ [rad]	a [m]	d [m]	α [rad]
0	0	0.16235	π/2
0	0.42517	0	0
0	-0.39239	0	0
0	0	0.13342	π/2
0	0	0.09955	-π/2
0	0	0.0996	0

The process model describes the physical behavior of the robot. The robot used in the experiments can be described by equation 6 using the direct dynamic to describe $\ddot{q}$.

$$\dot{x} = \begin{pmatrix} \dot{q} \\ \ddot{q} \\ \dddot{q} \end{pmatrix} = f(x, \tau, w) = \begin{pmatrix} \dot{q} \\ D(q, \dot{q}, \tau) \\ 0 \end{pmatrix} + w \tag{6}$$

Direct dynamics is a method in which the axis accelerations are calculated for a given axis angle, axis speed and axis drive torque based on the Lagrange formalism for dynamic motion equations. Which leads to:

$$\ddot{q} = M(q)^{-1}(\tau - C(q, \dot{q})\dot{q} - G(q) - F_r(\dot{q})) \tag{7}$$

This contains a mass matrix $M(q)$ describing the inertial forces and moments. Gyroscopic forces lead to the corresponding matrix $C(q, \dot{q})$. Frictional influences are considered by the vector $F_r(\dot{q})$. These can include, for example, static friction and viscous friction. The vector $G(q)$ considers gravitational influences on the axis segments. The driving moments of the axes are described by τ. [9] The model uncertainties are accounted for by the additive Gaussian noise w. This is assumed to be equally distributed for each axis, and the noise is given by w where each entry is a 6x1 vector:

$$w = (w_1 \quad w_2 \quad w_3)^T \tag{8}$$

Parameters of the dynamic equation were taken from [11]. Third deviation of axis angels, angular jerk Jerk $\dddot{q}$ is assumed to be constant between timesteps. Small changes of $\ddot{q}$ are modelled by third entry of the additive gaussian noise w_3.

The measurement model h(x) is given by:

$$h(x_k) = \begin{pmatrix} q \\ \dot{\rho} \\ \ddot{\rho} \end{pmatrix} + e_k \in \mathbb{R}^{12} \tag{9}$$

including axis angles q measured by axis encoder, cartesian velocity $\dot{\rho}$ measured by the OS for x- and y-direction and cartesian acceleration $\ddot{\rho}$ measured by IMU. As OS do not measure z-axis velocity it is modelled by a gaussian noise distribution due to planar motions in our experiments. Measurement noise e_k was determined by analysis of standstill measurements and given in Table 2.

Table 2 Sensor Noise Values.

Sensor	Noise Values		
	σ_X	σ_Y	σ_Z
IMU	$0.0116105\ m/s^2$	$0.0124071\ m/s^2$	$0.00990842\ m/s^2$
	σ_1	σ_2	σ_3
Encoder	$2.3678 \cdot 10^{-5}$ rad	$2.1291 \cdot 10^{-5}$ rad	$2.2662 \cdot 10^{-5}$ rad
	σ_4	σ_5	σ_6
	$2.5278 \cdot 10^{-5}$ rad	$2.2238 \cdot 10^{-5}$ rad	$2.5379 \cdot 10^{-5}$ rad
OS	σ_X	σ_X	
	$7 \cdot 10^{-3} m/s$	$7 \cdot 10^{-3} m/s$	

Covariance matrix of measurement noise given by

$$R_k = \begin{pmatrix} R_{ENC} & 0 & 0 \\ 0 & R_{OS} & 0 \\ 0 & 0 & R_{IMU} \end{pmatrix} \in \mathbb{R}^{12\times 12} \tag{10}$$

With the diagonal values being 3x3 diagonal matrices using the sensor noise values.

3.2 Evaluation Strategy

To evaluate the performance of the EKF, the measured reference trajectory of the LT is compared with the calculated trajectory of the EKF. Likewise, the RPD of the robot is compared with the reference measurement to validate the improvement of the position determination of the EKF. To evaluate the performance of the approach, three different parameters are collected. First, the Root-Mean-Square-Error (RMSE) between the trajectories is used. This is the averaged squared error between the points of the reference measurement (R) taken from the laser tracker system and the path to be evaluated (B) being either the EKF results or the RPD values. The standard deviation is determined from the absolute error of the individual points to be able to make a statement about the dispersion of the deviations. As a further evaluation parameter, the maximum absolute error (maxAE) is calculated. The parameters refer in each case to the coordinates x and y. An overview of the evaluation parameters and how they are calculated is given in Table 3.

Table 3 Performance Parameters.

Parameter	Calculation
RMSE	$\sqrt{\overline{(R-B)^2}}$
maxAE	$\max_i \lvert (R_i - B_i) \rvert$
Std.-Dev.	$\sqrt{\frac{1}{N-1}\sum_{i=1}^{N}\lvert((R_i-B_i)-\mu\rvert^2}$ $mit\ \mu = \overline{R-B}$

Evaluation parameters are averaged over all experimental iterations to reduce influence of systematic errors on results.

4. Results

The evaluation parameters RMSE and maxAE for the triangular path are shown for v_2 in Fig. 4. Parameters are listed for the EKF and RPD trajectories in x- and y-directions, respectively.

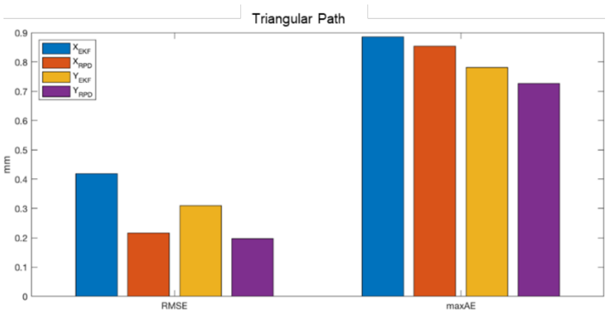

Fig. 4 RMSE and maxAE for triangular path.

An axial directional dependency is visible for EKF RMSE and maxAE values. Overall, values for EKF paths are higher than for RPD paths. In Table 4 standard deviations of EKF and RPD paths are depicted.

Table 4 Position error standard deviations for triangular paths.

	in mm at 50mm/s	var *in mm* at 150mm/s
X_{EKF}	$65.74 \cdot 10^{-3}$	$53.05 \cdot 10^{-3}$
X_{RPD}	$65.51 \cdot 10^{-3}$	$52.82 \cdot 10^{-3}$
Y_{EKF}	$66.17 \cdot 10^{-3}$	$53.33 \cdot 10^{-3}$
Y_{RPD}	$65.51 \cdot 10^{-3}$	$52.82 \cdot 10^{-3}$

In Fig. 5 position measurements of EKF, RPD and LT are depicted for one recorded motion at v_2 and zoomed in at the 90° angle of the triangle. Direction of motion is indicated with a red arrow.

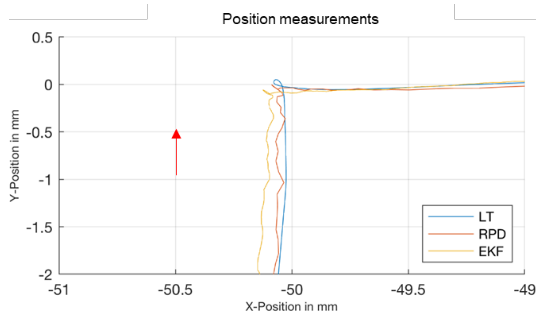

Fig. 5 Detailed section of triangular motion at v_2.

A displacement of the EKF path to the LT path x-axis direction is observable. Further, no overshoot after the abrupt direction change is observed. For v_1 similar observations were made. To investigate observed x-axis displacement closer, RPD, LT and results of the forward kinematic (FK) calculation done as part of the EKF estimation are depicted in Fig. 6.

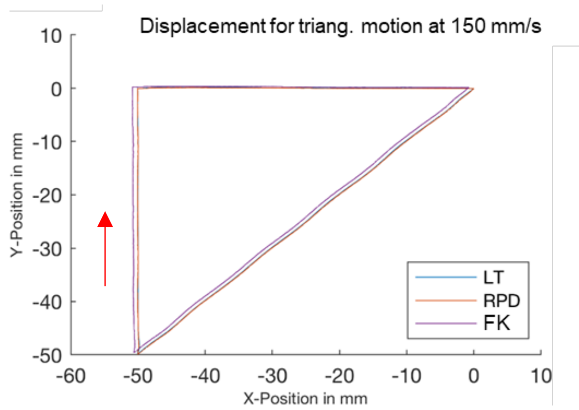

Fig. 6 Position from LT, RPD and FK for triangular motion at v_2.

In this global depiction of position a displacement is visible for FK positions in contrast to LT and RPD positions. To further investigate observed displacement errors relative distance measurements of OS are investigated by analyzing measured length of hypotenuse of triangular by comparison of OS and LT measured length. That way, x- and y- component of motion should be visible in individual measurements of optical sensors. Maximum position errors of 20mm at v_2 were observable.

For circular paths, performance parameters RMSE and maxAE are depicted in Fig. 7.

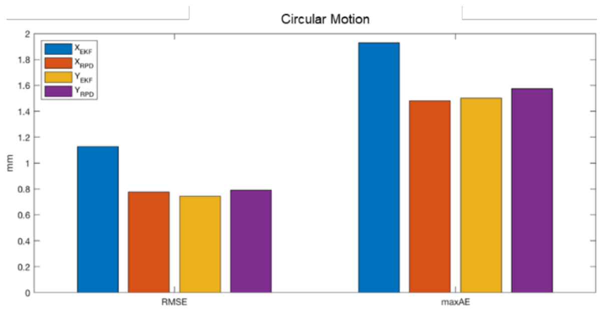

Fig. 7 RMSE and maxAE for circular path.

Axial directional dependency for EKF RMSE and maxAE values is observable for circular motions as well. RMSE and maxAE is only higher for x-axis direction, while in y-axis direction values are lower than for RPD paths. Standard deviations of EKF and RPD positions of circular paths are given in Table 5.

Table 5 Position error standard deviation for circular paths.

	Std. −Dev. *in mm* at 150mm/s
X_{EKF}	$794.56 \cdot 10^{-3}$
X_{RPD}	$794.37 \cdot 10^{-3}$
Y_{EKF}	$794.67 \cdot 10^{-3}$
Y_{RPD}	$794.37 \cdot 10^{-3}$

Error standard deviation differs by less then 0.1% for circular paths. Evaluation parameters RMSE and maxAE are depicted in Fig. 8.

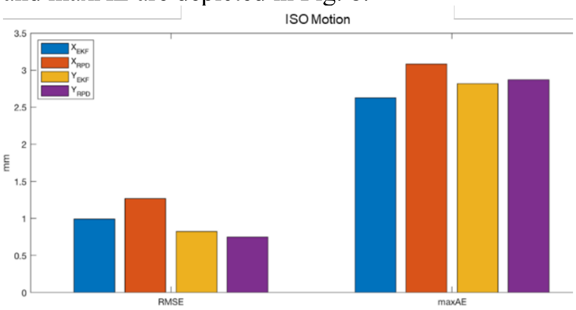

Fig. 8 RMSE and maxAE for ISO path.

Axial direction dependency is observable for EKF performance parameters. But in contrast to previously introduced results, dependency is not similarly distinct in RMSE and maxAE. For RMSE x-Axis values are higher while they are higher in y-axis direction for maxAE. The ISO trajectory generated by the EKF is 10% more accurate relative to the RMSE. The maxAE is also 9% lower. In Table 5 position standard deviations for iso paths are depicted.

Table 6 Position error standard deviation for iso paths.

	Std. −Dev. *in mm* at 150mm/s
X_{EKF}	$54.17 \cdot 10^{-3}$
X_{RPD}	$54.89 \cdot 10^{-3}$
Y_{EKF}	$53.94 \cdot 10^{-3}$
Y_{RPD}	$54.89 \cdot 10^{-3}$

In Fig. 9 a detailed ISO path between waypoints 28 and 31 (see Fig. 4) at v_2 is depicted. Positions of LT, EKF and RPD are presented. Direction of motion is given with a red arrow.

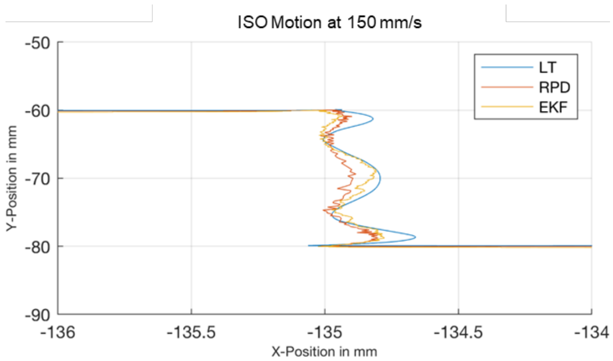

Fig. 9 Detailed section ISO motion between waypoints 28 and 31 at v_2.

5. Discussion

Analysis of the results reveals several key findings. Firstly, when considering triangles, higher root mean square error (RMSE) and maximum errors were observed. Similarly, similar errors were visible in the forward kinematics (FK) results indicating that displacement of FK positions has a significant influence on the estimation results and suggesting that the error source lies in the FK modeling. Potential reasons for these errors could be unknown offsets for axis positions or an error-prone implementation of FK when using the robotics toolbox.

However, despite these errors, there was a lower difference in standard deviation between EKF and RPD results for iso paths observable, indicating that dispersion of position estimations around the estimated path can be on same scale or even lower for EKF estimations. This suggests that while absolute errors may be high, the shape of the trajectory is estimated at a similar level to the RPD. Additionally, when examining circular paths, similar results were observed, with higher RMSE in the x-direction, which can be attributed to the displacements observed in triangular paths. Furthermore, the known anisotropic behavior of the IRs could contribute to axial-dependent errors if not adequately modeled in the process model.

Measurement errors from the optical sensor were found to be relatively high when the motion was not in the measurement direction. However, for motions in one measurement direction with deviations orthogonal to that, the estimation results of EKF were better than RPD, as demonstrated in Fig. 9. Comparing the ISO trajectory, the errors were close to or even lower than the RPD, indicating overall lower standard deviation and more stable results. The advantage of the EKF approach was particularly observable for the ISO path in Fig. 9, as it provided better estimation of overshoot and resulting dominant oscillations induced by dynamic motions such as direction changes.

7. Conclusion

In conclusion, the sensor fusion approach did not significantly increase position estimation accuracy in a relevant order of magnitude. This outcome can be attributed to two major reasons that have been identified. Firstly, the high influence of forward kinematic errors need for their correction in future approaches to fully analyze performance of the SF approach and impact of FK calculations on performance. It is crucial to explore and compare alternative implementations of FK to determine the most effective approach. However, it is worth noting that when the motion is solely in the measurement direction of a one-dimensional sensor, the results demonstrate potential for improved position estimation capability compared to RPD. Used optical sensors did create high errors when motion was not solely in direction of measurement. To fully exploit this potential across a variety of motions, it is necessary to test and incorporate other sensors for relative tool speed measurements into the concept. Promising results for tool speed measurement have been observed with speckle-based sensors [12]. Nevertheless, the potential for improvement is visible, particularly for the ISO trajectory, as the estimated overshoot and resulting oscillation were better estimated with the EKF than with the RPD. By employing alternative sensors and adopting a different forward kinematic (FK) modeling approach, it is plausible to achieve better results in future studies. Further research is warranted to explore the integration of new tool speed sensors and refine the FK modeling. This would enable a comprehensive investigation of their impact on the overall performance of the sensor fusion approach.

Acknowledgments and Appendixes

(1) Funded by the Deutsche Forschungsgemeinschaft (DFG, German Research Foundation) under Germany s Excellence Strategy – EXC-2023 Internet of Production – 390621612.

(2) The authors acknowledge the financial support by the Federal Ministry of Education and Research of Germany in the framework of Research Campus Digital Photonic Production (project number: 13N15423).

References

[1] R. Poprawe: “Digital Photonic Production - The Future of Laser Applications”, LIA TODAY, (2015), p. 14.

[2] Optech Consulting: online available at: https://optech-consulting.com/2021_laser_market_data, (2022).

[3] C. Möller: „Entwicklung eines hochgenauen Bearbeitungsroboters durch den Einsatz zusätzlicher Messtechnik“, (Hamburg, 2019), p.35.

[4] J. Bremer, P. Walderich, N. Pirch, J. H. Schleifenbaum, A. Gasser, and T. Schopphoven: J. Laser Appl., 33, (2021) 012045.

[5] D. L. Hall and J. Llinas: Proc. of the IEEE, 85, (1997) 6.

[6] T. Emter: „Integrierte Multi-Sensor-Fusion für die simultane Lokalisierung und Kartenerstellung für mobile Robotersysteme.“, (Publisher, KIT Scientific Publishing Karlsruhe, 2021), p.235.

[7] F. Caron, E. Duflos, D. Pomorski and, P. Vanheeghe: J. Info. Fusion, 7, (2006) 221.

[8] J. Mareczek: „Modellbildung von Kinematik und Dynamik.“ (Publisher, Springer Vieweg, Berlin, 2020), p. 82.

[9] B. Siciliano: “Robotics: Modelling, planning and control. “ (Publisher: Springer, London, 2009), p. 40.

[10] L. Cen and S. N Melkote: J. Procedia Manufact., 10, (2017) 486.

[11] P. Boscariol, R. Caracciolo, D. Richiedei and, A. Trevisani: Appl. Sci., 10, (2020) 3022.

[12] T. O.H. Charrett, Y. K. Bandari, F. Michel, J. Ding, S. W. Williams, and R. P. Tatam: J. Rob. and Comp.-Integ. Mfg., 53, (2018) 187.

[13] KEBA Industrial Automation GmbH: online available at: https://www.keba.com/de/news/industrial-automation/robotergenauigkeit, (2022).

(Received: July 4, 2023, Accepted: February 12, 2024)